JACC: BASIC TO TRANSLATIONAL SCIENCE VOL. 10, NO. 1, 2025

ORIGINAL RESEARCH - PRECLINICAL

TIMD4^{hi}MHCII^{hi} Macrophages Preserve Heart Function Through Retnla

Danyang Zhang, PhD,[a,b,c,*] Xuanhao Wang, PhD,[a,b,c,*] Lianlian Zhu, MS,[a,b,c] Yuxing Chen, PhD,[a,b,c] Chao Yang, PhD,[a,b,c] Zhiwei Zhong, MS,[a,b,c] Xiangming Kong, MS,[a,b,c] Jinliang Nan, PhD,[a,b,c] Chen Wang, PhD,[a,b,c] Hengxun Hu, PhD,[a,b,c] Jinghai Chen, PhD,[a,d] Peng Shi, PhD,[a,d] Xinyang Hu, MD, PhD,[a,b,c,e] Wei Zhu, PhD,[a,b,c] Jian'an Wang, MD, PhD[a,b,c,e]

VISUAL ABSTRACT

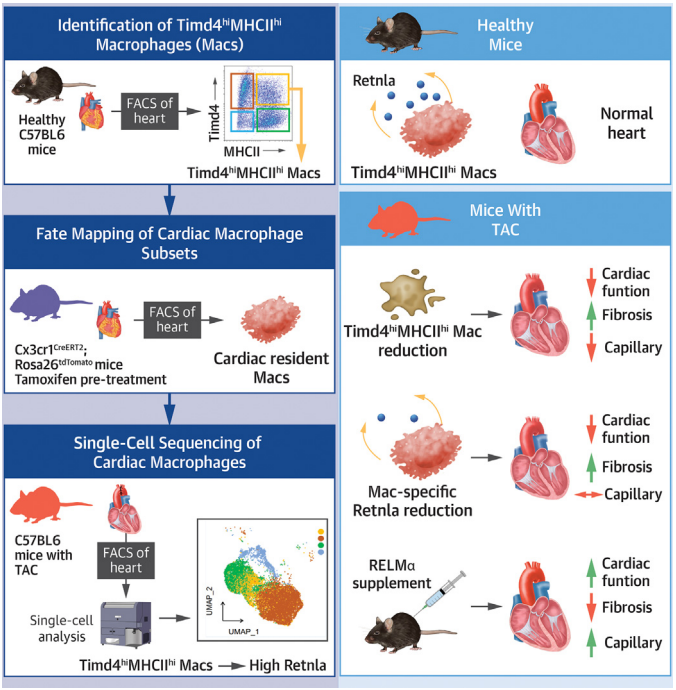

Zhang D, et al. JACC Basic Transl Sci. 2025;10(1):65-84.

HIGHLIGHTS

- **Genetic fate mapping has confirmed the existence of the TIMD4^{hi}MHCII^{hi} macrophage subset, demonstrating that they were resident macrophages with minimal contribution from peripheral monocytes.**
- **In the pressure overload-induced heart failure mouse model, TIMD4^{hi}MHCII^{hi} macrophages exhibited a significant and distinct reduction in their numbers during the late heart failure stage.**
- **Single-cell RNA sequencing identified *Retnla* as the signature gene for TIMD4^{hi}MHCII^{hi} macrophages.**
- **Administration of recombinant protein of the *Retnla* gene, RELMα, delayed the onset of heart failure. In contrast, either deletion of TIMD4^{hi}MHCII^{hi} macrophages or the specific loss of *Retnla* in macrophages accelerated the progression of heart failure.**

From the [a]Department of Cardiology, Second Affiliated Hospital, School of Medicine, Zhejiang University, Hangzhou, Zhejiang, China; [b]State Key Laboratory of Transvascular Implantation Devices, Hangzhou, Zhejiang, China; [c]Cardiovascular Key Laboratory of Zhejiang Province, Hangzhou, Zhejiang, China; [d]Institute of Translational Medicine, Zhejiang University School of Medicine, Hangzhou, Zhejiang, China; and the [e]Research Center for Life Science and Human Health, Binjiang Institute of Zhejiang University, Hangzhou, Zhejiang, China. *Dr Zhang and Dr X. Wang contributed equally to this work and are joint first authors.
The authors attest they are in compliance with human studies committees and animal welfare regulations of the authors' institutions and Food and Drug Administration guidelines, including patient consent where appropriate. For more information, visit the Author Center.

Manuscript received May 24, 2024; revised manuscript received August 15, 2024, accepted August 26, 2024.

ISSN 2452-302X https://doi.org/10.1016/j.jacbts.2024.08.009

JACC: BASIC TO TRANSLATIONAL SCIENCE VOL. 10, NO. 1, 2025
JANUARY 2025:65–84

ABBREVIATIONS AND ACRONYMS

AAV = adeno-associated virus

AMI = acute myocardial infarction

DCM = dilated cardiomyopathy

DN = TIMD4 and MHCII double negative

DP = TIMD4 and MHCII double positive

DT = diphtheria toxin

E = embryonic day

EF = ejection fraction

FS = left ventricular fractional shortening

IP = intraperitoneally

LVEF = left ventricular ejection fraction

PBS = phosphate-buffered saline

scRNA-seq = single-cell RNA sequencing

TAC = transverse aortic constriction

TAVR = transcatheter aortic valve replacement

SUMMARY

Genetic fate mapping confirmed the existence of the TIMD4^{hi}MHCII^{hi} macrophage subset and showed that they were resident macrophages with minimal input from peripheral monocytes. Further, single-cell RNA sequencing revealed that *Retnla* could serve as the signature gene for TIMD4^{hi}MHCII^{hi} macrophages. Administration of recombinant protein of the *Retnla* gene, RELMα, delayed the onset of heart failure, whereas either deletion of TIMD4^{hi}MHCII^{hi} macrophages or macrophage-specific loss of *Retnla* facilitated heart failure progression. (JACC Basic Transl Sci. 2025;10:65–84)

Macrophages reside in different organ tissues throughout the body[1] and play essential roles in maintaining homeostasis and processing inflammatory responses to various stress conditions.[2-8] Within the heart, cardiac resident macrophages can be divided into CCR2^{-} and CCR2^{+} subsets based on the CCR2 (C-C chemokine receptor 2) expression level, and these subsets are derived from embryonic and adult hematopoietic lineages, respectively.[9-11] Studies have shown that embryonic-derived CCR2^{-} macrophages protect against adverse remodeling, whereas adult-derived CCR2^{+} macrophages exacerbate the heart failure process.[12-16] Similar studies have been carried out in a small group of end-stage heart failure patients who received a left ventricle assist device followed by sex-mismatched heart transplants, highlighting the distinct functions of macrophages from dichotomous origins.[17]

Single-cell RNA sequencing (scRNA-seq) analysis further classified the CCR2^{-} tissue-resident macrophages into 2 distinct subgroups based on the expression of TIMD4 (the phosphatidylserine receptor T-cell immunoglobin and mucin domain containing 4) and MHCII (major histocompatibility complex II). The 2 distinct resident macrophage subpopulations—namely, TIMD4^{hi}MHCII^{lo} macrophages and TIMD4^{lo}MHCII^{hi} macrophages—coexist across the tissue and have been shown to have unique spatial locations and exert specialized functions.[18-21] Although a significant amount of detailed information has been provided in these studies at the single-cell level, additional functional studies are needed to further understand each macrophage subpopulation's roles.

A special TIMD4^{hi}MHCII^{hi} macrophage subpopulation was detected in our initial flow cytometry graph, which was also detected in the previously published single-cell sequencing data,[13,16] and here we name this subgroup of macrophages the double-positive (DP) macrophages. Interestingly, however, little is known about this macrophage subset. In the present study, we aimed to investigate the biology of this DP macrophage population in various organs/tissues in the mouse. Using the genetic fate mapping technique combined with the bone marrow transplant chimera mouse model, we also carefully described the origin and lifecycle dynamics of this DP macrophage subset compared to TIMD4^{hi}MHCII^{lo} and TIMD4^{lo}MHCII^{hi} macrophages, the well-known cardiac resident macrophage subsets. We specifically targeted the DP macrophage subgroup by using an orthogonal recombinase approach, which allowed us to assess the functional role of the DP macrophage subset in vivo, specifically in the pressure overload-induced heart failure mouse model. Importantly, our scRNA-seq data have identified *Retnla* as a unique marker gene for the DP macrophage subset, and we validated that knockdown of its expression in macrophage cells using the Cx3cr1^{CreERT2};Retnla$^{flox/flox}$ mouse model resulted in a worsening of cardiac performance. Meanwhile, DP macrophage reduction also significantly decreased *Retnla* levels, which was associated with augmented pathologic remodeling. Finally, supplementing with recombinant RELMα improved cardiac performance, thus highlighting the essential role of Retnla and DP macrophages in cardiac function.

METHODS

STUDY DESIGN. This study aimed to systematically investigate macrophage subpopulations and compare DP macrophages with TIMD4^{hi} and MHCII^{hi} macrophage subsets. Age- and sex-matched C57BL/6, Rosa26$^{CAG-GFP}$, Cx3cr1^{CreERT2};Rosa26^{tdTomato}, Rosa26$^{CAG-LSL-RSR-tdTamoto-2A-DTR}$, and Cx3cr1^{creERT2};Retnla$^{flox/flox}$ mice were used for this research. Genetic and pharmacologic approaches were used to evaluate the roles of DP macrophages in a nonischemic

cardiomyopathy model. scRNA-seq analysis of macrophages guided our exploration of the mechanisms underlying DP macrophage function. Furthermore, we collected human heart tissues to compare mouse and human macrophage subsets. For each experiment, n values are specified in the corresponding figure legends and were predetermined for each experiment based on expected biological and technical variability.

HUMAN SAMPLES. Normal heart samples were collected from brain-dead donors (Supplemental Table 1). Plasma samples were collected before and 1 month after transcatheter aortic valve replacement (TAVR) surgery among patients with severe aortic stenosis. For patients with acute myocardial infarction (AMI), plasma samples were collected before percutaneous coronary intervention. Plasma samples were collected after admission for patients with dilated cardiomyopathy (DCM) (Supplemental Table 2). Age- and sex-matched patients with normal coronary angiography and heart function served as the control group. We excluded patients with diabetes, malignant tumors, autoimmune diseases, and infections to minimize the impact on resistin results. Informed consent was obtained from all patients or their legal guardians. The study was approved by the Human Research Ethics Committee of the Second Affiliated Hospital of Zhejiang University School of Medicine. The heart specimens were embedded in optimal cutting temperature compound and stored at -80 °C. Plasma samples were also stored at -80 °C until analysis. Clinical characteristics of donors and DCM patients are shown in Supplemental Table 1. Clinical characteristics of the TAVR, AMI, and DCM patients are shown in Supplemental Table 2.

MICE AND TREATMENT. Cx3cr1^{CreERT2} (strain no. 021160), CD45.1 (strain no. 002014), and Rosa26^{tdTomato} mice (strain no. 007909) were procured from Jackson Laboratory. Cx3cr1^{CreER2} mice were crossed with Rosa26^{tdTomato} mice to generate Cx3cr1^{CreER2}; Rosa26^{tdTomato} mice. Rosa26$^{CAG\text{-}LSL\text{-}RSR\text{-}tdTamoto\text{-}2A\text{-}DTR}$ and Retnla$^{flox/flox}$ mice were constructed, respectively, by Shanghai Southern Model Organisms and GemPharmatech, using CRISPR/Cas9 technology on the background of C57BL/6J mice. Wild-type C57BL/6 mice were purchased from Shanghai Slac Model Organisms. Mice were bred in the animal facility at Zhejiang University. Mice were housed in a temperature- and humidity-controlled specific pathogen-free facility with a 12-hour light/dark cycle and ad libitum access to water and standard laboratory rodent chow. All animal experiments were approved by the Animal Ethics Committee of the Second Affiliated Hospital of Zhejiang University School of Medicine, Hangzhou, China. For fate mapping, 100 mg of tamoxifen (Sigma-Aldrich) was added into 10 mL of corn oil and sonicated at 37 °C while rocking until dissolved. The 3- or 4-week-old Cx3cr1^{CreER2}; Rosa26^{tdTomato} mice and Cx3cr1$^{CreER\text{-}T2}$;Retnla$^{flox/flox}$ mice were injected intraperitoneally (IP) with tamoxifen for 10 days (50 mg/kg every other day). For reconstitution of RELMα, 10 mg of bacteria-expressed RELMα (Peprotech) was injected IP twice a week for 4 weeks.

BONE MARROW CHIMERAS. The schematic strategy to generate CD45.1-CD45.2 chimeric mice was as follows: recipient CD45.2 mice were sublethally irritated to their head and chest, performed with a lead shield, followed by transplantation via tail vein injection of bone marrow cells from CD45.1 donor mice. The resulting chimera mice carried 50% CD45.2$^+$ and 50% CD45.1$^+$ cells in the blood but only had CD45.2$^+$ resident cardiac macrophages.

MINIMALLY INVASIVE TRANSVERSE AORTIC CONSTRICTION MODEL IN MICE. Minimally invasive transverse aortic constriction (TAC) in mice with very low operative and postoperative mortalities has been described in detail in the previous literature.[22] Briefly, mice aged 8 to 10 weeks were anesthetized with isoflurane. Following a 3- to 4-mm upper partial sternotomy, a segment of 6/0 silk suture was threaded through the eye of a ligation aid and then passed under the aortic arch and tied over a blunted 27-gauge needle. Sham-operated animals underwent the same surgical preparation but without aortic constriction.

FLOW CYTOMETRY AND GATING STRATEGY. Detailed methods, including the antibodies used, can be found in Supplemental Materials and Methods (Supplemental Table 3). Analysis software (FlowJo) was used to analyze flow cytometric data. The complete gating strategies of tissue macrophages are shown in Supplemental Figure 1 and are described in the Supplemental Materials and Methods.

IMMUNOFLUORESCENCE STAINING. Hearts were isolated at reported times and fixed in 4% paraformaldehyde for 2 hours, followed by a 30% sucrose gradient overnight. The tissue was embedded in optimal cutting temperature compound medium (Sakura Finetek) and flash-frozen in isopentane suspended in liquid nitrogen. The tissue was sectioned into 6-μm slices at 2 cutting levels. The sections were blocked for 30 minutes and permeabilized for 5 minutes with 5% bovine serum (Sigma-Aldrich) and 0.01% Triton X (Sigma-Aldrich) in phosphate-buffered saline (PBS), respectively. The sections were washed with PBS, and the primary antibody

(listed in Supplemental Table 2) was added overnight at 4 °C in a hydrated chamber. The sections were then washed with PBS and labeled with secondary antibodies diluted in PBS for 30 minutes at room temperature. Finally, the sections were mounted with Antifade Mounting Medium with 4′,6-diamidino-2-phenylindole (Vectorlabs) and imaged on the LSM980 confocal microscope (Zeiss) using a 20× or 40× objective lens.

ECHOCARDIOGRAPHY. Transthoracic echocardiography was performed using a Vevo 2100 system (VisualSonics), as previously described.[23] Briefly, mice were anesthetized by isoflurane inhalation. A comprehensive echocardiographic study, during which 2-dimensional and M-mode images were acquired and analyzed, was performed to assess cardiac morphology and function.

IN VIVO ADENO-ASSOCIATED VIRUS DELIVERY. Recombinant adeno-associated virus (AAV) that contained a vector encoding Cre under the promotor driven by Lyve1 and the AAV that contained a vector encoding Dre under the promotor of MHCII were generated (Hanbio Inc). Five-week-old Rosa26$^{CAG\text{-}LSL\text{-}RSR\text{-}tdTamoto\text{-}2A\text{-}DTR}$ mice were anesthetized by isoflurane, and mixed AAV solutions (3.2×10^{11} and 2.4×10^{11} vector genomes per mouse, respectively) were injected directly into the myocardium of the left ventricle and apex region. The chest was closed, and the mice were extubated by spontaneous breathing and observed until they were fully awake.

To reduce DP macrophages, diphtheria toxin (DT) (List Biological Laboratories) was diluted in PBS and administered to mice IP acutely (25 ng/mg body weight) or chronically (25 ng/mg every other day for 4 weeks).

SINGLE-CELL RNA SEQUENCING. Cell sorting was performed using Aria instrumentation (BD Bioscience). Live single immune cells (4′,6-diamidino-2-phenylindole-CD45$^+$) were gated and were sorted directly into Dulbecco's modified Eagle medium plus 50% bovine serum for scRNA-seq using the 10× Genomics platform. The package Seurat (version 4.0.3) was used for all scRNA-seq analyses using R 4.0.3. We used the slingshot package (2.12.0) to analyze the trajectories of DP, Lyve1^{hi}, or MHCII^{hi} macrophage subpopulations. Details are described in the Supplemental Appendix.

STATISTICS. Data are presented as mean ± SEM unless otherwise specified. A 2-tailed Student's *t*-test was used to compare the differences between the 2 groups. One-way or 2-way analysis of variance combined with the Tukey post hoc test for multiple pairwise comparisons was used to compare 3 or more groups. Repeated-measures analysis of variance or paired Student's *t*-tests were used to compare longitudinal changes within a group. Linear regression analysis was used for the association of 2 continuous variables with the Pearson correlation coefficient (*r*) provided. The Shapiro-Wilk normality test was used to determine that data were normally distributed. Statistical significance was defined as $P < 0.05$. Statistics were performed using Prism 7 software (GraphPad Software).

RESULTS

ONTOGENY AND DYNAMICS OF THE TIMD4^{hi}MHCII^{hi} MACROPHAGE SUBGROUP IN THE HEART. To validate and further characterize the DP macrophage population in the heart, we isolated CD45$^+$CD11b$^+$CD64$^+$ cells from mouse hearts with the C57BL/6J gene background and performed flow cytometry based on their expression levels of TIMD4 and MHCII. We have detected 4 macrophage subgroups: TIMD4^{hi}MHCII^{lo} macrophages (referred to as TIMD4^{hi} macrophages), TIMD4^{lo}MHCII^{hi} macrophages (MHCII^{hi} macrophages), DP macrophages, and TIMD4^{lo}MHCII^{lo} macrophages (double-negative [DN] macrophages). These 4 groups of macrophages accounted for 31.34% ± 4.16%, 26.87% ± 6.09%, 25.22% ± 4.65%, and 7.04% ± 1.96% of total cardiac macrophages, respectively (Figure 1A).

To further clarify the lifecycle dynamics for each macrophage subset, we quantified each cluster of cardiac macrophages obtained from different ages of mice at embryonic day (E) 12.5 and E17.5 as well as at 1, 7, 14, 28, 42, 56, 168, 336, and 504 days after birth (Figure 1B). We demonstrated that at E12.5, when most CD64$^+$CD11b$^+$ macrophages in the heart were DN macrophages, the absolute number of DN macrophages continued to increase at the embryonic stage E17.5 and reached its peak at 1 day after birth. The number of DN macrophages then showed a gradual decrease throughout the lifecycle. Meanwhile, TIMD4^{hi} macrophages showed a moderate number at E12.5, accounting for 23.26% ± 0.12% of the total cardiac macrophages, and showed a moderate increase at 28 days after birth. However, the number decreased at the end of our observation period, that is, day 504 after birth. In contrast, both the DP and MHCII^{hi} macrophage subpopulations were first detected at 28 days after birth, increased at 42 days after birth, and maintained their populations at this level at 168 days after birth. However, the DP macrophage population showed a slight decrease in

FIGURE 1 **TIMD4^{hi}MHCII^{hi} MΦs Were Present in the Heart During the Lifecycle**

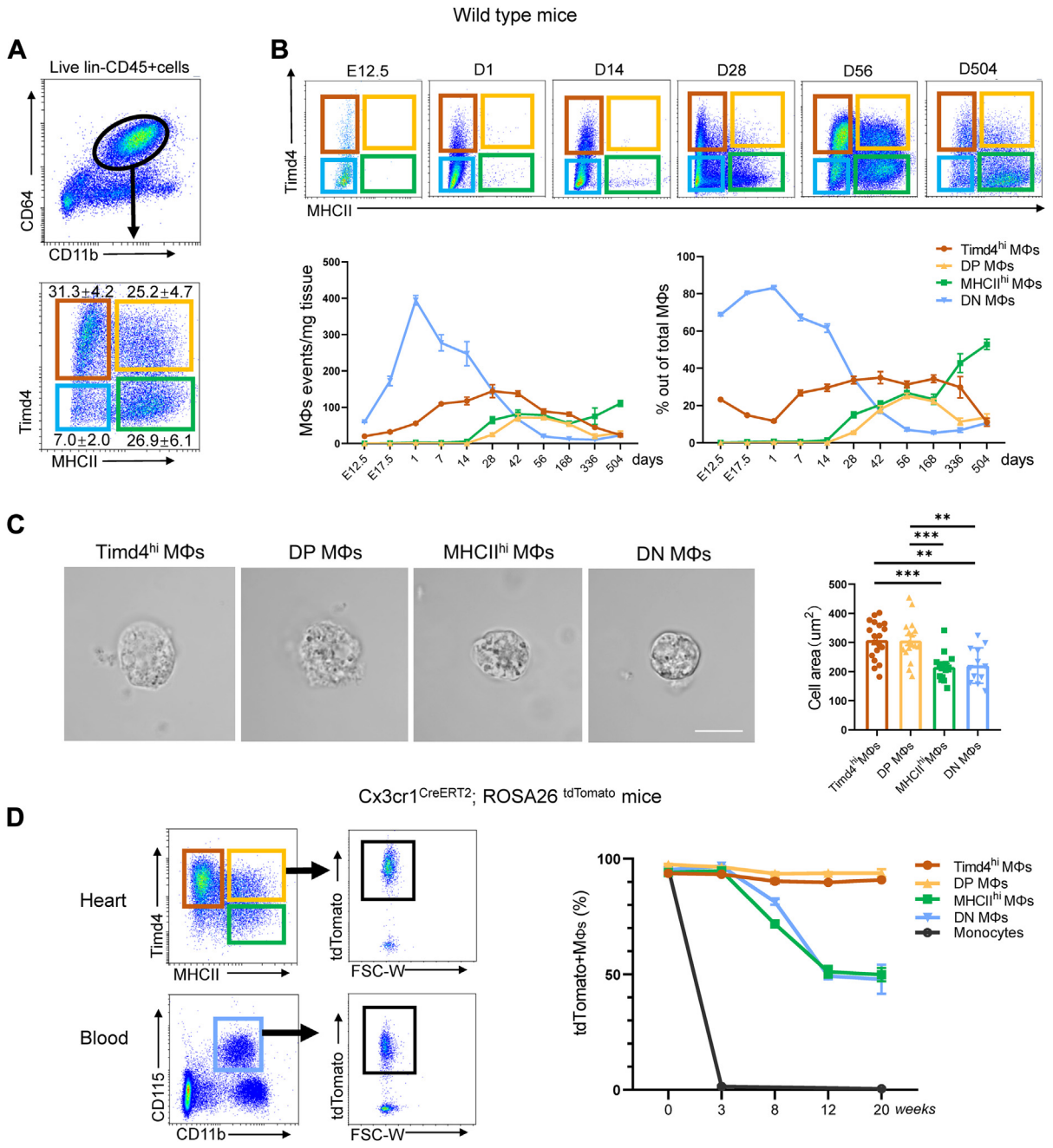

(A) The gating strategy of flow cytometry. After CD45 screening, the CD11b-positive and CD64-positive cells were gated and subjected to further analysis for their expression of TIMD4 and MHCII (top). Representative flow cytometric analysis plots showing the 4 macrophage subsets—namely, TIMD4^{hi} (in the red square), DP (in orange), MHCII^{hi} (in green), and DN (in blue) MΦs (bottom). (B) With the same flow cytometry strategy, the time course of changes in the number of the 4 MΦ subsets in the heart tissue isolated from mice of different ages was analyzed (representative plots of different ages shown in top row). The percentage (lower left) or absolute number (lower right) for each MΦ subset was also quantified, demonstrating the unique dynamics for each subset (n = 2-6 experiments using up to 8 mice per timepoint). (C) Representative images showing the morphology of TIMD4^{hi}, DP, and MHCII^{hi} MΦs freshly isolated from the hearts (left) with the cell size quantified and shown in the bar graph (right). Scale bar: 10 μm. The experiments for each group consisted of 17 to 27 biological replicates obtained from 2 or 3 mice. Values were analyzed by using analysis of variance with Tukey post hoc analysis. (D) Recombination rates of cardiac MΦs are expressed as the percentage of tdTomato labeling for each MΦ subset after tamoxifen administration, of which the percentage of labeling was evaluated at different timepoints up to 20 weeks. All numeric data are expressed as the mean ± standard error of the mean. $^{**}P < 0.01$; $^{***}P < 0.001$. D = day; DN = double negative; DP = double positive; E = embryonic day; MΦ = macrophage.

FIGURE 2 Identification of DP MΦs Across Tissues

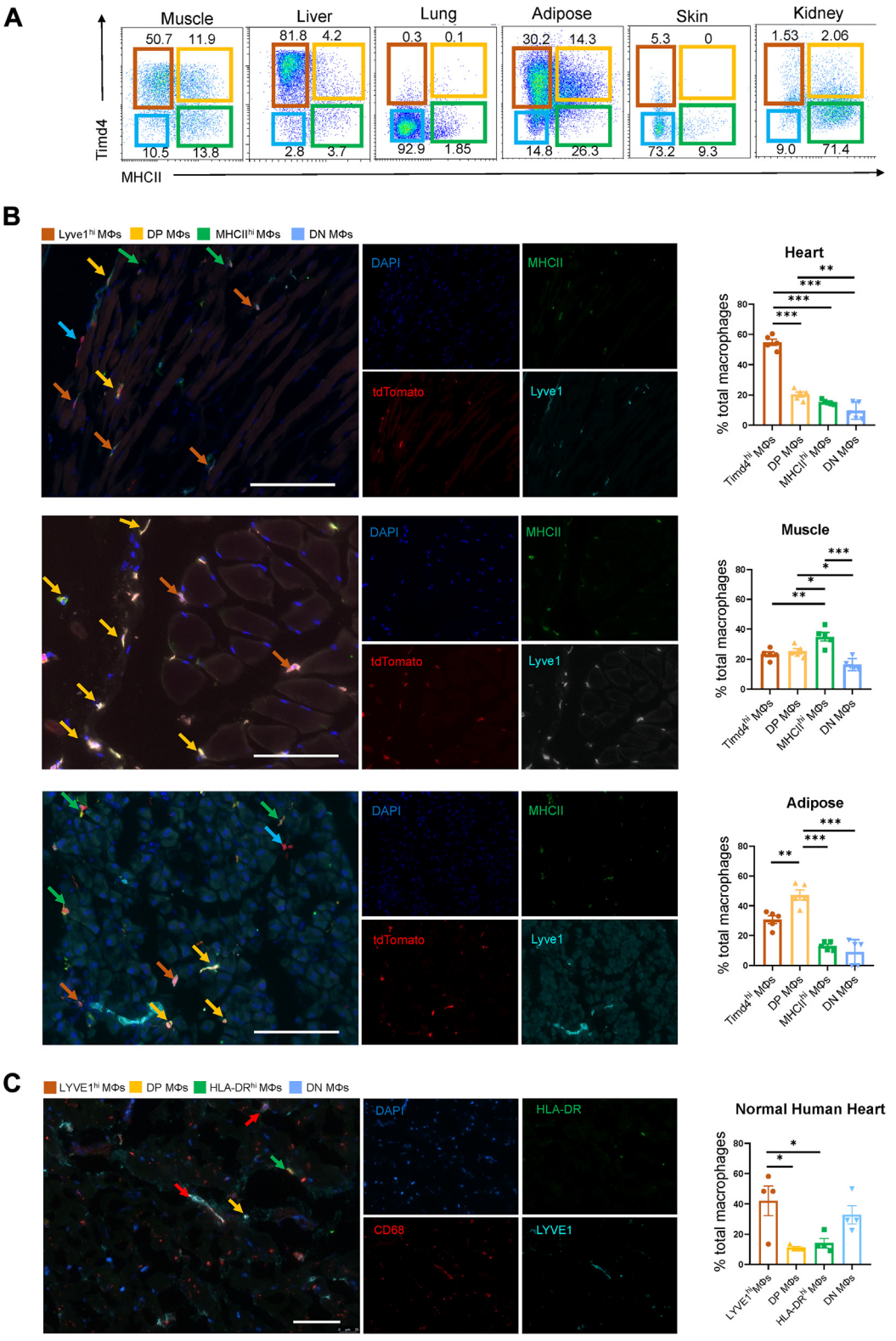

Continued on the next page

its number afterward, whereas the MHCII^{hi} macrophages gradually increased (Figure 1B).

Different cardiac macrophage subsets were also analyzed using a confocal microscope after isolation and sorting by flow cytometry. The cross-sectional areas of both TIMD4^{hi} and DP macrophages were larger than those of MHCII^{hi} macrophages. To characterize the phagocytosis capacity of the macrophage subpopulations, we isolated tdTomato-labeled macrophages from the heart tissue of Cx3cr1^{CreER2};Rosa26^{tdTomato} mice treated with tamoxifen. In parallel, the hearts of Rosa26$^{CAG\text{-}GFP}$ mice were also digested to obtain GFP-positive cardiac cells, which were exposed to UV irradiation to generate GFP^{+} cardiomyocytes (GFP^{+} apoptic cardiomyocytes) that underwent apoptosis. The tdTomato^{+} macrophages were then cocultured with GFP^{+} apoptic cardiomyocytes to examine the phagocytosis of each macrophage subset. Flow cytometry showed that the tdTomato^{+}GFP^{+} cell proportion was the highest in the TIMD4^{hi} macrophage subgroup after 4 hours of coculture, suggesting that TIMD4^{hi} macrophages had the most robust phagocytosis capacity compared with DP or MHCII^{hi} macrophages (Supplemental Figure 1A).

DP MACROPHAGE POPULATIONS WERE SELF-MAINTAINED WITH MINIMAL INPUT FROM BLOOD MONOCYTES. We also used Cx3cr1^{creERT2};Rosa26^{tdTomato} mice, which allowed for conditionally fate mapping Cx3cr1^{+} macrophages (Supplemental Figures 1B and 1C) following tamoxifen delivery. After tamoxifen delivery (50 mg/kg, IP injection), more than 95% of the circulating monocytes were positively labeled with tdTomato, whereas more than 90% of the CD45^{+}CD11b^{+}CD64^{+} macrophages isolated from the heart were tdTomato^{+} immediately post-tamoxifen treatment (Figure 1D). After 3 weeks of tamoxifen withdrawal, the circulating monocytes were replenished with freshly derived bone marrow progenitors and became negatively labeled with tdTomato (Figure 1D), whereas 95% of DP macrophages within the heart remained tdTomato^{+} (Figure 1D), and this percentage almost remained the same as the mice aged (Figure 1D). Consistent with previous reports,[16] the rate of TIMD4^{hi} macrophages that were tdTomato^{+} was 93% at 3 weeks after tamoxifen withdrawal and did not change significantly when re-evaluated at 20 weeks after withdrawal (Figure 1D). However, this percentage of tdTomato^{+} cells among MHCII^{hi} macrophages was 86% and 65% at 3 and 20 weeks after tamoxifen withdrawal, respectively. Thus, the gradual decrease in the percentage of tdTomato-labeled cells in MHCII^{hi} macrophages suggested input from peripheral monocytes. In contrast, no significant changes in the percentages of tdTomato-positive TIMD4^{hi} and DP macrophages indicated no monocyte input, exhibiting different inherent dynamics (Figure 1D).

To gain insights into the proliferation abilities of different macrophage subsets, bromodeoxyuridine (BrdU) was injected IP into mice 2 hours before sampling. Flow cytometry was used to measure the proportion of macrophages in the S phase (BrdU^{+}) to evaluate proliferation activity. Our findings indicated that the percentages of BrdU^{+} cells within the TIMD4^{hi}, DP, and MHCII^{hi} macrophage subset were 0.66%, 1.21%, and 0.38%, respectively (Supplemental Figure 1D). These data demonstrated that the proliferative capacity of the DP macrophage subgroup was akin to that of the TIMD4^{hi} macrophage subgroup, exhibiting a moderate self-proliferation capability to maintain the population at a steady state. In contrast, MHCII^{hi} macrophages displayed a relatively lower proliferative activity, which is consistent with the fact that they can receive input from peripheral monocytes to maintain their population.

IDENTIFICATION OF DP MACROPHAGES ACROSS TISSUES. To investigate the DP macrophages in other organs, the tissues of skeletal muscle, liver, lung, fat, skin, and kidney were collected from C57/BL6 mice to isolate the macrophages. Using the same gating strategy described earlier (Figure 1A), DP macrophages were detected in skeletal muscle and adipose tissue, which comprised 11.9% and 14.3% of the total number of macrophages, respectively. DP macrophages can also be detectable in the liver and kidney but at a very low level, and they were not detected in the lung (interstitial macrophages) or skin tissues (Figure 2A).

FIGURE 2 Continued

(A) Skeletal muscle, liver, lung, fat, skin, and kidney tissues were obtained from adult Cx3cr1^{CreERT2};Rosa26^{tdTomato} mice, and single cells were then isolated and prepared for flow cytometry. Data were obtained from 2 or 3 mice. (B) Immunofluorescence staining images and quantification of MΦ subsets per 20× field of view in heart, adipose, and skeletal muscle tissues from Cx3cr1^{CreERT2};Rosa26^{tdTomato} mice. Scale bar: 100 μm. The percentage of MΦ subsets among the total MΦs was calculated (n = 5 from 2 or 3 mice; 2 experiments). Values were analyzed by using analysis of variance with Tukey post hoc analysis. (C) Immunofluorescence staining images and quantification of MΦ subsets per 20× field of view in the interventricular septum of normal human heart samples. Macrophages were divided into 4 subpopulations—namely, LYVE1^{hi}HLA-DR^{lo}, LYVE1^{hi}HLA-DR^{hi}, LYVE1^{lo}HLA-DR^{hi}, and LYVE1^{lo}HLA-DR^{lo} MΦs. Scale bar: 50 μm. All numeric data are expressed as the mean ± SEM, *P < 0.05; **P < 0.01; ***P < 0.001. DAPI = 4′,6-diamidino-2-phenylindole; ns = not statistically significant; other abbreviations as in Figure 1.

FIGURE 3 Pressure Overload Stress Drove Dynamic Changes in Cardiac DP Macrophages

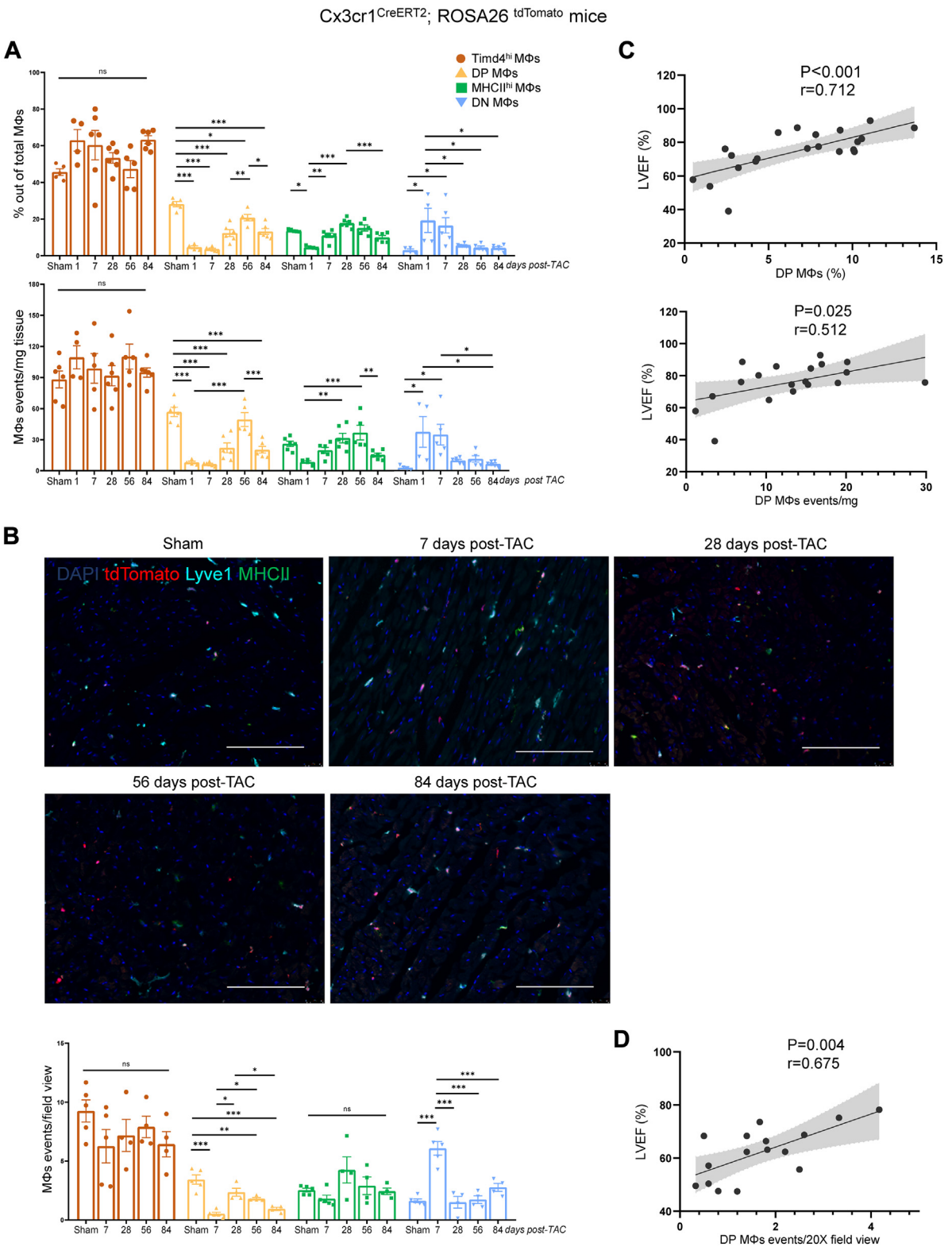

Continued on the next page

Immunofluorescence analysis was also carried out, and an antibody against LYVE1 was used because it can reliably label TIMD4^{hi} macrophages, according to the previous report.[21] We observed the coexistence of the 3 macrophage subtypes—TIMD4^{hi}/LYVE1^{hi} macrophages, MHCII^{hi} macrophages, and DP macrophages—in the heart, skeletal muscle, and adipose tissues (**Figure 2B**).

To further investigate the DP macrophages in human heart tissues, we studied formalin-fixed human heart tissue samples from donors with normal hearts. Immunofluorescence staining was performed explicitly on the interventricular septum. We found that cardiac macrophages in human hearts can be similarly categorized into 4 subgroups based on the LYVE1 and HLA-DR markers: LYVE1^{hi}HLA-DR^{lo}, LYVE1^{hi}HLA-DR^{hi}, LYVE1^{lo}HLA-DR^{hi}, and LYVE1^{lo} HLA-DR^{lo} macrophages (**Figure 2C**).

PRESSURE OVERLOAD STRESS DROVE DYNAMIC CHANGES IN CARDIAC DP MACROPHAGES. To assess the biological function of these cardiac DP macrophages, we further analyzed their dynamic changes under pathologic conditions, particularly during the progression of heart failure. We used a TAC mouse model, which displays a distinct transition from compensatory myocardial hypertrophy in the early phase to decompensated heart failure in the late phase.

We aimed to study the dynamics of macrophage subgroups at both the acute phase (1 day post-TAC)—that is, the initial compensatory cardiac hypertrophy stage (7 and 28 days post-TAC)—and the late decompensated heart failure stage (56 and 84 days post-TAC) (**Figure 3A**). Although the TIMD4^{hi} macrophages exhibited a trend of increase in the numbers at either the early (1 and 7 days post-TAC) or late (84 days post-TAC) stage, this did not reach statistical significance. On the other hand, the DP subgroup exhibited a decrease in number at 1 and 7 days post-TAC, whereas the MHCII^{hi} subgroup only showed a reduction at 1 day post-TAC. Both subgroups subsequently demonstrated a gradual recovery in their numbers, with the MHCII^{hi} subgroup returning fully to its basal level at 56 days post-TAC. In contrast, full recovery was not observed for the DP subgroup. Notably, in the late decompensated heart failure phase (ie, 84 days post-TAC), the number of DP macrophages plummeted to nearly half of that at the basal level, whereas MHCII^{hi} macrophages showed only a minor reduction at this terminal heart failure stage. In contrast, the proportion of the TIMD4^{hi} subgroup within the cardiac macrophages remained unchanged compared to the basal stage (sham-operated mice) (**Figure 3A**, top). The same pattern of changes was observed when the data were expressed in terms of the absolute number per weight of heart tissue (**Figure 3A**, bottom).

We also performed immunofluorescence staining using heart tissue obtained at each timepoint following TAC, as described earlier; a similar pattern of changes was detected for the 3 distinct macrophage subgroups. It is noteworthy that, with both flow cytometry and immunofluorescence staining, the DN macrophage subgroup initially showed a sharp increase at the early stage, which, however, then subsided at the late stage, exhibiting no differences compared to the basal level (**Figure 3B**).

To confirm the changes in the dynamics of each cardiac macrophage subgroup, a CD45.1-CD45.2 chimera mouse model was also established (Supplemental Figure 2A). Flow cytometry analysis was used to quantify the ratio of CD45.1^{+} cells to CD45.2^{+} cells in cardiac macrophages, which was also adjusted by peripheral blood monocyte chimerism. We deduced the monocyte input ratio for each cardiac macrophage subset (Supplemental Figure 2B). The DP macrophage subgroup was then quantified in terms of both the percentage proportion and absolute quantity, which recapitulated the same pattern of changes, as shown in the data obtained from Cx3cr1^{CreERT2};ROSA26^{tdTomato} mice (Supplemental Figure 2C).

FIGURE 3 Continued

Either the TAC or sham procedure was performed with the Cx3cr1^{CreERT2};Rosa26^{tdTomato} mice at 3 weeks after the completion of tamoxifen administration. Cardiac cells were isolated from the heart tissues and subjected to flow cytometry analysis. (A) The percentage (top) and absolute number (bottom) of each MΦ subset were quantified and expressed relative to the total macrophage population and per milligram of cardiac tissue, respectively (n = 4-6 per timepoint). (B) Representative immunofluorescence staining images (top) and quantification of macrophage subsets (bottom) per 20× field of view in heart tissues. Scale bar: 100 μm (n = 4 or 5 randomized paraffin-embedded sections per timepoint). Values in A and B were analyzed using analysis of variance with Tukey post hoc analysis. (C, D) Linear regression analysis was carried out to assess the association between the number of DP MΦs acquired by (C) flow cytometry or (D) immunofluorescence staining and the left ventricular ejection fraction acquired by echocardiography. Dashed lines indicate 95% CIs (n = 16-19). All the data are expressed as the mean ± SEM. *$P < 0.05$; **$P < 0.01$; ***$P < 0.001$. LVEF = left ventricular ejection fraction; TAC = transverse aortic constriction; other abbreviations as in **Figures 1 and 2**.

DP MACROPHAGES HAD INSUFFICIENT PHAGOCYTOSIS-DERIVED PROLIFERATION ABILITY. By analyzing the ratio of tdTomato-positive cells within each macrophage subset, we could evaluate to what extent the recruitment of tdTomato-negative blood monocytes contributed to each macrophage subpopulation (Supplemental Figure 3A). We showed that the percentage of tdTomato-positive cells within the TIMD4^{hi} macrophage subgroup remained constant throughout the observation period post-TAC, and the number within the DP macrophage subgroup only experienced a slight decrease at 7 days post-TAC, which rapidly returned to the basal level and remained at the level for the remaining observation period. In contrast, for the MHCII^{hi} macrophage subgroup, this number decreased significantly (35.17%) at 7 days post-TAC and recovered (65.83%) at 28 days post-TAC. With heart failure further progressing, the tdTomato-positive-labeled MHCII^{hi} macrophages again gradually lost their population number, with the percentage reaching a nadir of 18.77% at 84 days post-TAC surgery (Supplemental Figure 3A), indicating a significant input from the circulating monocytes. A similar pattern of changes was found in the CD45.1-CD45.2 chimera mouse model (Supplemental Figure 2D).

Macrophages maintain their population through self-proliferation, peripheral monocyte input, or both. To quantify the proliferation capability for each macrophage subgroup, we treated mice with BrdU at different times to quantify the proliferating cell percentage among each macrophage subset. Interestingly, in the basal state (ie, the sham-operated mouse hearts), the DP subset showed slightly higher proliferative activity than the other subsets (Supplemental Figure 1D). Of note, at 1 day post-TAC, each subset showed a trend of increase in the number of BrdU-labeled cells but without reaching statistical significance. At 7 days post-TAC, TIMD4^{hi} macrophages had the most significant increase in their proliferation activity, showing the highest percentage of BrdU-positive labeled cells, and both the DP and MHCII^{hi} macrophage subsets also exhibited substantial increases in their proliferation ability, although to a relatively low extent (Supplemental Figure 3B). Therefore, we reason that because the DP macrophage subset did not receive much input from peripheral monocytes, this relatively low proliferation activity inherent to the DP macrophages was not sufficient to maintain their population, which also explains the fact that this population experienced a reduction in its number at the following timepoints. Notably, the increased proliferative activity of all subsets soon returned to basal levels at the later decompensated heart failure stage (Supplemental Figure 3B).

A previous study demonstrated that a higher proliferation rate of macrophages was usually associated with the phagocytosis capacity.[24] We hypothesized that a higher phagocytic capacity of TIMD4^{hi} macrophages in the acute phase was associated with their stronger proliferative capacity, which accounts for a stable quantity of TIMD4^{hi} macrophage numbers under stress. We further demonstrated in the present study that TIMD4^{hi} macrophages have stronger phagocytic capacity in vitro (Supplemental Figure 1A) and proliferative activity in vivo (quantification of BrdU-labeled macrophages is shown in Supplemental Figure 3B) than either DP or MHCII^{hi} macrophages. To confirm the relationship between phagocytosis and proliferation, we measured the proliferation rates of the 3 macrophage subpopulations at 4 hours and 24 hours after stimulation of phagocytosis in vitro. We showed that these 3 macrophage subpopulations had a significantly elevated percentage of 5-Ethynyl-2'-deoxyuridine (EdU)-positive cells 4 hours after phagocytosis stimulation (Supplemental Figure 3C). At 24 hours after phagocytosis induction, we found that the EdU-positive ratio of TIMD4^{hi} macrophages increased further, whereas both DP and MHCII^{hi} macrophages did not show any further increase in the ratio of positive EdU labeling (Supplemental Figure 3C). Thus, our data support the hypothesis that the induction of phagocytosis promoted the proliferation process, which was evident in the TIMD4^{hi} macrophage subpopulation. We also infer that the dramatic reduction in the DP macrophage population was probably related to their limited phagocytosis, and this was not the case for MHCII^{hi} macrophages, because they received input from peripheral monocytes.

SPECIFIC REDUCTION OF DP MACROPHAGES ACCELERATED THE HEART FAILURE REMODELING PROCESS. We have shown that DP macrophages, but not TIMD4^{hi} or MHCII^{hi} macrophages, exhibited a significant decrease in the absolute number at the late decompensated heart failure stage compared with the sham group (**Figures 3A and 3B**, Supplemental Figure 2C). We evaluated the relationship between DP macrophages and heart systolic function during this decompensation process (4-12 weeks post-TAC surgery). We quantified the DP macrophages in the heart with flow cytometry (**Figure 3C**) and immunofluorescence staining (**Figure 3D**) and assessed their relationship to the heart function obtained before the mice were sacrificed. The results demonstrated that the number of DP macrophages was significantly reversely related to the ejection fraction (EF) value

(**Figures 3C and 3D**). We then aimed to test whether the reduction of DP macrophages can disrupt cardiac homeostasis and, hence, impair cardiac performance. To specifically manipulate the DP macrophage population, we applied orthogonal recombinase systems. Rosa26$^{CAG\text{-}LSL\text{-}RSR\text{-}tdTomato\text{-}2A\text{-}DTR}$ (Rosa26 $^{LSL\text{-}RSR\text{-}tdT\text{-}DTR}$) mice were constructed with the CRISPR/CAS-9 approach, which allows expression of both tdTomato and DTR receptors only when both Cre and Dre enzymes are expressed. The AAV that contained the vector encoding Cre under the promotor driven by Lyve1 and the AAV that contained the vector encoding Dre under the promotor of MHCII were generated separately and injected directly into the myocardium of Rosa26 $^{LSL\text{-}RSR\text{-}tdT\text{-}DTR}$ mice simultaneously to clear cells expressing both LYVE1 and MHCII. Rosa26 $^{LSL\text{-}RSR\text{-}tdT\text{-}DTR}$ mice that received empty AAV served as controls (**Figure 4A**). We found that DT delivery significantly decreased the percentage of the DP macrophage subset in the total macrophage population in Rosa26 $^{LSL\text{-}RSR\text{-}tdT\text{-}DTR}$ mice (from 25.21% before to 19.7% after DT delivery to the Rosa26 $^{LSL\text{-}RSR\text{-}tdT\text{-}DTR}$ mice) (**Figure 4B**), although at a relatively smaller amount. A similar pattern of changes was observed when the absolute number of DP macrophages was quantified (48.18 events/mg in response to AAV compared to 32.91 events/mg) after DT treatment compared with placebo therapy (**Figure 4B**). Immunofluorescence staining using the heart tissue that was exposed to the AAV injection showed that approximately 53.19% ± 12.43% of DP macrophages were labeled as tdTomato^{+} cells (Supplemental Figure 4A). Meanwhile, there was minimal overlap between tdTomato^{+} cells and lymphatic vessels (Supplemental Figures 4B and 4C), suggesting that very few lymphocytes were labeled with tdTomato. Importantly, during the process of induction of DP macrophage reduction, we did not detect any significant changes in lymphocyte and neutrophil infiltration or the expression levels of the proinflammatory cytokines Il1b, Tnfa, Il6, and Ccl2 in cardiac tissue (Supplemental Figures 4D and 4F and Supplemental Table 4) at the basal status, and cardiac morphology (cardiac chamber size and fibrosis formation) and performance were not affected (**Figure 4C**, Supplemental Figure 4E).

We then subjected these mice that received AAV injection within the heart to the TAC surgical procedure, and the DT therapy started 1 day before TAC surgery and continued twice a week for 4 consecutive weeks (**Figure 4A**). Echocardiography examination showed that DP macrophage reduction resulted in a decrease in cardiac function as early as 7 days post-TAC, as evidenced by the changes in the left ventricular EF (LVEF) (DP reduced group: 57.13% vs control group: 66.73%) and fractional shortening (FS) (DP reduced group: 53.16% vs control group: 70.64%). Although the left ventricular size remained the same as that in the basal state at 7 days post-TAC, the ventricle was significantly dilated at 28 days post-TAC compared with Rosa26$^{LSL\text{-}RSR\text{-}tdT\text{-}DTR}$ mice treated with empty AAV (**Figure 4C**). Moreover, there were no significant differences in either the cardiomyocyte area or vascular density between the 2 groups (**Figures 4E and 4F**). However, fibrosis in the DP macrophage-reduced group was significantly increased (**Figure 4D**).

scRNA-SEQ REVEALED THAT DP MACROPHAGES HAD HIGH EXPRESSION OF *RETNLA*. To further understand the differences between DP macrophages and other macrophage subpopulations, cardiac CD45^{+} immune cells were sorted from mice in the sham group, mice at 7 days post-TAC therapy, and mice at 9 weeks post-TAC (for the chronic decompensated heart failure stage). Single-cell transcriptomic analysis was performed using the 10× Genomics platform. The sham, 1 week post-TAC, and 9 weeks post-TAC data sets were first merged using the merge function in Seurat and then were preprocessed and filtered for all subsequent analyses (Supplemental Figures 5A and 5B). To assess the functional state of cardiac macrophages (Supplemental Figures 5C and 5D), we calculated the module score of cells belonging to the *Lyve1*^{hi} cluster, *MHCII*^{hi} cluster, and monocyte clusters gained by unsupervised clustering using the AddModuleScore function (Supplemental Figure 5E). The top 10 genes for the *Lyve1*^{hi} and *MHCII*^{hi} clusters were chosen. We defined these 2 gene sets as input for the AddModuleScore function and named them "Lyve1score" and "MHCIIscore," respectively. Then, we applied the kmeans function to the scaled matrix containing the Lyve1score and MHCIIscore of cells in the *Lyve1*^{hi} and *MHCII*^{hi} clusters and projected all cells into 2-dimensional space (Supplemental Figure 5F). We named cells lying in the left regions as "*Lyve1*^{hi} macrophages." The cells in the right lower region were defined as "*MHCII*^{hi} macrophages," and the cells in the right upper region were defined as "*Lyve1*^{hi}*MHCII*^{hi} macrophages" (Supplemental Figure 5G). *Lyve1*^{hi}*MHCII*^{hi} macrophages had relatively high expression levels of both *Lyve1* and *MHCII* (Supplemental Figure 5H).

We used the "FindMarkers" function to compute the differentially expressed genes of 3 macrophage clusters relative to monocytes (**Figure 5A**). *Lyve1*-^{hi}*MHCII*^{hi} macrophages highly expressed *Retnla* and

FIGURE 4 Specific Reduction of DP MΦs Accelerated the Transition to Heart Failure

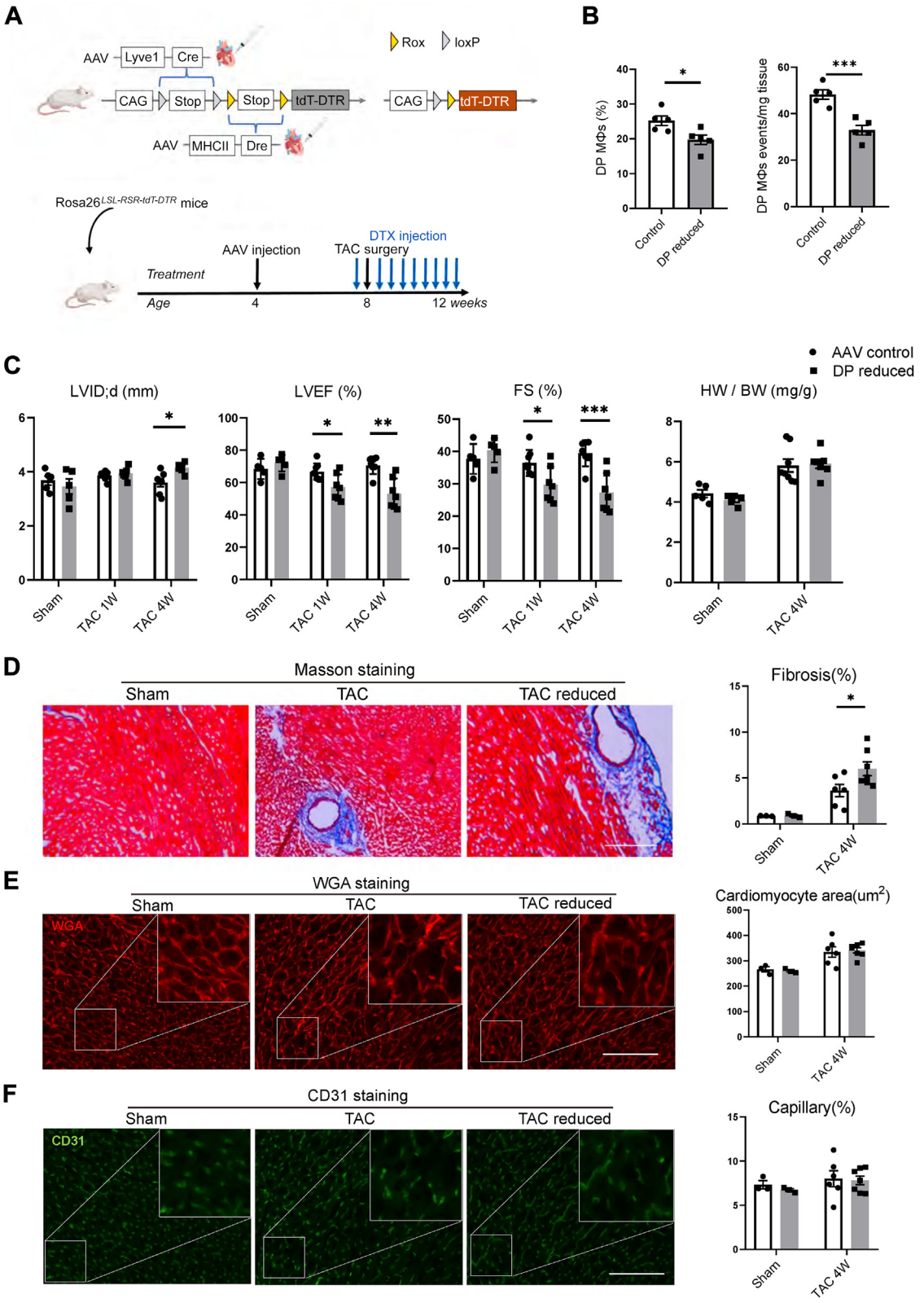

Continued on the next page

Mgl2 compared with the other 2 subpopulations, which was consistent with previous single-cell sequencing data (**Figure 5B**, Supplemental Figure 5I).[25] The percentage of *Lyve1*^{hi}*MHCII*^{hi} macrophages decreased at 1 week post-TAC and 9 weeks post-TAC compared with that in the sham group (**Figure 5C**), consistent with data acquired by flow cytometry (**Figure 3A**). We also compared cardiac macrophage gene expression across conditions and found that *Retnla* expression showed a significant decrease in either the 1 week post-TAC or 9 weeks post-TAC hearts compared with sham-operated hearts (**Figure 5D**). Macrophages from mouse heart tissue were isolated, and the *Retnla* expression level was quantified using flow cytometry. Compared to the other 2 subsets (TIMD4^{hi} or MHCII^{hi} macrophages), the ratio of Retnla-positive cells in DP macrophages was the highest (**Figure 5E**). Specifically, the expression levels of both *Retnla* and *Mgl2* were significantly reduced in DP macrophage-reduced hearts, supporting the notion that DP macrophages served as a major source of *Retnla* in the heart (**Figure 5F**). The decrease in *Retnla* levels was also consistent with the fact that the DP macrophage subgroup underwent sharp decreases in its numbers at both the early acute compensatory and late decompensated heart failure stages.

The gProfiler was used to measure the overrepresentation of our defined gene list against the Gene Ontology database. The predicted pathways of the macrophages from the sham group included metabolism processes and angiogenesis. In contrast, the macrophages of hearts 1 week post-TAC were enriched in immune system processes and cell activation because of the acute pressure stress condition (**Figure 5G**). Interestingly, macrophages within hearts 9 weeks post-TAC were enriched in programmed cell death or apoptotic processes (**Figure 5G**). We also used the slingshot package to analyze the trajectories of *Lyve1*^{hi}*MHCII*^{hi}, *Lyve1*^{hi}, or *MHCII*^{hi} macrophage subpopulations. We found that *Lyve1*^{hi}*MHCII*^{hi} macrophages might differentiate into *MHCII*^{hi} macrophages (Supplemental Figure 5J).

SELECTIVE LOSS OF RESIDENT MACROPHAGE–DERIVED *RETNLA* EXACERBATED CARDIAC DYSFUNCTION. We next sought to evaluate whether the expression level of *Retnla* influences pathologic cardiac remodeling. Cx3cr1^{CreERT2};Retnla$^{flox/flox}$ mice were created, in which *Retnla* derived from resident macrophages was conditionally reduced upon tamoxifen administration. We validated the model by detecting decreased *Retnla* protein expression of cultured bone marrow–derived macrophages from Cx3cr1^{CreERT2}; Retnla $^{flox/flox}$ mice compared with Retnla$^{flox/flox}$ mice (**Figure 6A**). We also performed flow cytometry to assess the expression of *Retnla* in macrophage subpopulations and found that it was effectively knocked down in all 3 subsets without affecting the components or numbers in the macrophage population (Supplemental Figures 6A to 6C). Of note, reducing *Retnla* levels in Cx3cr1-expressing cells led to increased insulin sensitivity without significant weight change (Supplemental Figures 6D and 6E).

We then subjected mice that received tamoxifen treatment to the TAC surgery, and an echocardiography examination was performed every 4 weeks (**Figure 6B**). The conditional *Retnla* reduction mice demonstrated decreased cardiac function at 12 weeks post-TAC, as evidenced by the changes in both the LVEF (*Retnla* reduction group: 50.63% vs control group: 64.36%) and FS (*Retnla* reduction group: 27.30% vs control group: 38.70%) (**Figure 6C**). Moreover, there were no significant differences in the cardiomyocyte cross-sectional area between the 2 groups (**Figure 6E**). However, fibrosis in the *Retnla*-reduced group was significantly increased, accompanied by less density of vessels (**Figures 6D and 6F**), indicating an impaired angiogenesis process.

FIGURE 4 Continued

(A) AAV that contained a vector encoding Cre under the promotor driven by Lyve1 and the AAV that contained a vector encoding Dre under the promotor of MHCII (DP reduced) or empty AAV (control) were injected directly into the myocardium of Rosa26$^{LSL\text{-}RSR\text{-}tdT\text{-}DTR}$ mice (top). Schematic of the generation of the DP MΦ reduction mouse model where diphtheria toxin administration was delivered 1 day before TAC surgery and continued at a dose of twice a week for 4 consecutive weeks (bottom). (B) The percentage (left) and absolute number (right) of DP MΦs in the left ventricle of the heart were measured by flow cytometry 3 days after diphtheria toxin administration (n = 5). (C) Echocardiography was performed to assess cardiac performance before TAC as a baseline and at 7 and 28 days post-TAC surgery (n = 5-8). (D-F) Fibrosis (measured by Masson staining; 5× field of view scale; scale bar: 300 μm), cardiac hypertrophy (measured by wheat germ agglutinin; 20× field of view; scale bar: 100 μm), and capillary (measured by CD31 staining; 20× field of view; scale bar: 100 μm) were assessed in sham-operated hearts and hearts obtained from mice at 28 days post-TAC, respectively (5-7 randomized visual fields were selected and analyzed for each heart and averaged; n = 5-7). All data are expressed as the mean ± standard error of the mean. Values were analyzed using Student's *t*-test unless otherwise specified. *$P < 0.05$; **$P < 0.01$; ***$P < 0.001$.
AAV = adeno-associated virus; DTX = diphtheria toxin; FS = left ventricular fractional shortening; HW/BW = heart weight/body mass ratio to assess cardiac hypertrophy; LVID = left ventricular end-diastolic diameter; W = weeks; WGA = wheat germ agglutinin; other abbreviations as in **Figures 1 to 3**.

FIGURE 5 Single-Cell RNA Sequencing Revealed That DP MΦs Had High Expression of *Retnla*

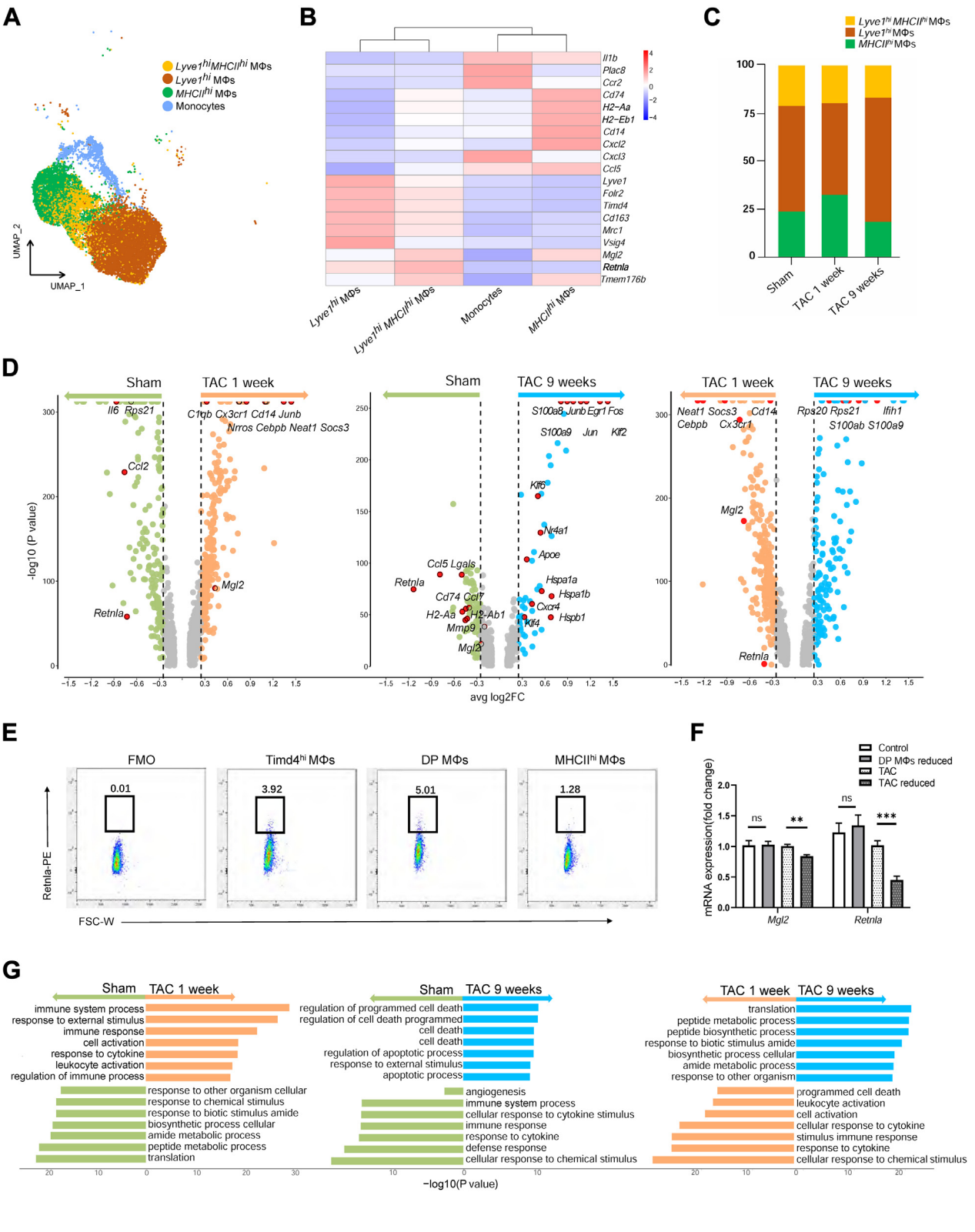

Continued on the next page

SUPPLEMENTATION WITH RECOMBINANT RELMα PREVENTED THE HEART FAILURE PROCESS. Given the data obtained from the Cx3cr1^{CreERT2};Retnla$^{flox/flox}$ mouse model, we aimed to test whether supplementation of RELMα, also known as FIZZ1, the protein that is encoded by the *Retnla* gene and found initially to be highly expressed in M2 macrophages,[25-27] could compensate for the loss of DP macrophage numbers and modulate the progression of heart failure. We supplemented the mice with recombinant RELMα IP, as previously described, twice a week from 6 to 9 weeks post-TAC (**Figure 7A**).[28] The timepoint was chosen based on our flow cytometry data when the number of DP macrophages was reduced while cardiac function was deteriorating. RELMα administration itself did not affect the number of DP macrophage populations in the heart tissue (Supplemental Figure 7A), and neither the level of blood glucose nor body weight was interrupted over our observation period (Supplemental Figures 7B and 7C).

After the completion of RELMα administration, cardiac function improved significantly, as evidenced by the increases in both LVEF and FS measured by echocardiography (**Figure 7B**). In addition, RELMα therapy decreased the ratio of heart weight to body weight (**Figure 7B**) but not heart weight itself. Of note, this enhanced cardiac function was also accompanied by less fibrosis (**Figure 7C**) and increased angiogenesis (**Figure 7E**). Importantly, the cardiomyocyte size did not show significant changes (**Figure 7D**). Further, we confirmed in vitro experiments that RELMα supplementation could significantly inhibit the fibrosis process (Supplemental Figures 7D and 7F) and promote angiogenesis in the tube formation assay (Supplemental Figure 7G) but did not affect cardiomyocyte hypertrophy (Supplemental Figure 7E).

These results highlight the role of RELMα as a major effector or mediator, largely secreted by DP macrophages, in regulating heart function by promoting angiogenesis and reducing the formation of fibrosis.

HUMAN PLASMA RESISTIN EFFECTIVELY PREDICTED RAPID HEART FUNCTION CHANGE. To further explore the clinical application value of resistin, a secreted protein that exhibits a distribution and function similar to that of Retnla in mice, we enrolled patients with AMI, patients with severe aortic stenosis, and patients with DCM. Our study revealed significantly elevated plasma resistin concentrations in patients with myocardial infarction and severe aortic stenosis as compared to the control group (**Figures 7G and 7H**). Conversely, DCM patients exhibited lower plasma resistin concentrations relative to the control group (**Figure 7I**). Further investigation revealed a significant correlation between the plasma resistin level and the cardiac function (EF value) in patients with myocardial infarction (**Figure 7J**). However, this unique correlation was insignificant among TAVR and DCM patients (data not shown). In patients with heart failure caused by aortic stenosis, 1 month after surgery, when their heart function significantly improved, we noted that the plasma levels of resistin had increased considerably in the majority of these patients (**Figure 7K**).

DISCUSSION

The essential protective roles of resident macrophages in the heart during both physiologic and pathophysiologic stress conditions have been well recognized.[3,5,29-32] However, the differential roles between different resident macrophage subgroups have not been specifically investigated. In our present study, we have detected and further examined the biological functions of the DP macrophage subcluster, especially their potential roles in pathologic processes in heart failure. Several important scientific questions need to be discussed and emphasized.

First, we identified and validated the DP macrophage subgroup. Although this cluster of macrophages has already been noticed in previous

FIGURE 5 Continued

Cardiac CD45^{+} immune cells were sorted from the sham group, 1 week post-TAC group (acute stress phase), and 9 weeks post-TAC group (chronic heart failure phase), and single-cell transcriptomic analysis was performed using the 10X Genomics platform. (A) Uniform manifold approximation and projection dimensionality reduction analysis identified that mononuclear MΦs consisted of *Lyve1^{hi}* MΦs, *Lyve1^{hi}MHCII^{hi}* MΦs, *MHCII^{hi}* MΦs, and monocytes after reclustering under "Lyve1score" and "MHCIIscore" dimensions. (B) Nineteen representative differentially expressed genes are plotted as a heatmap. (C) The percentage of MΦ subsets among the total MΦs across conditions. (D) Volcano plots of differentially expressed genes across conditions including both up-regulated and down-regulated genes (minimum percentage: 0.1; logFC threshold: 0.1; adjusted *P* value < 0.05). Genes of interest are highlighted in red. (E) The percentage of Retlna-positive cells among the MΦ subsets detected with flow cytometry. (F) The relative expression levels of *Retnla* and *Mgl2* in heart tissues were measured by quantitative polymerase chain reaction 3 days after diphtheria toxin injection between the sham and TAC groups (4 weeks post-TAC) using a DP MΦ–reduced model (TAC reduced). Values were analyzed by using analysis of variance with Tukey post hoc analysis. (G) Pathway enrichment analysis (gProfiler, Gene Ontology biological processes) using differentially expressed genes across conditions. $^{**}P < 0.01$; $^{***}P < 0.001$. avg = average; FC = fold change; mRNA = messenger RNA; other abbreviations as in **Figures 1 to 3**.

FIGURE 6 Selective Reduction of Resident Macrophage-Derived *Retnla* Exacerbated Cardiac Dysfunction

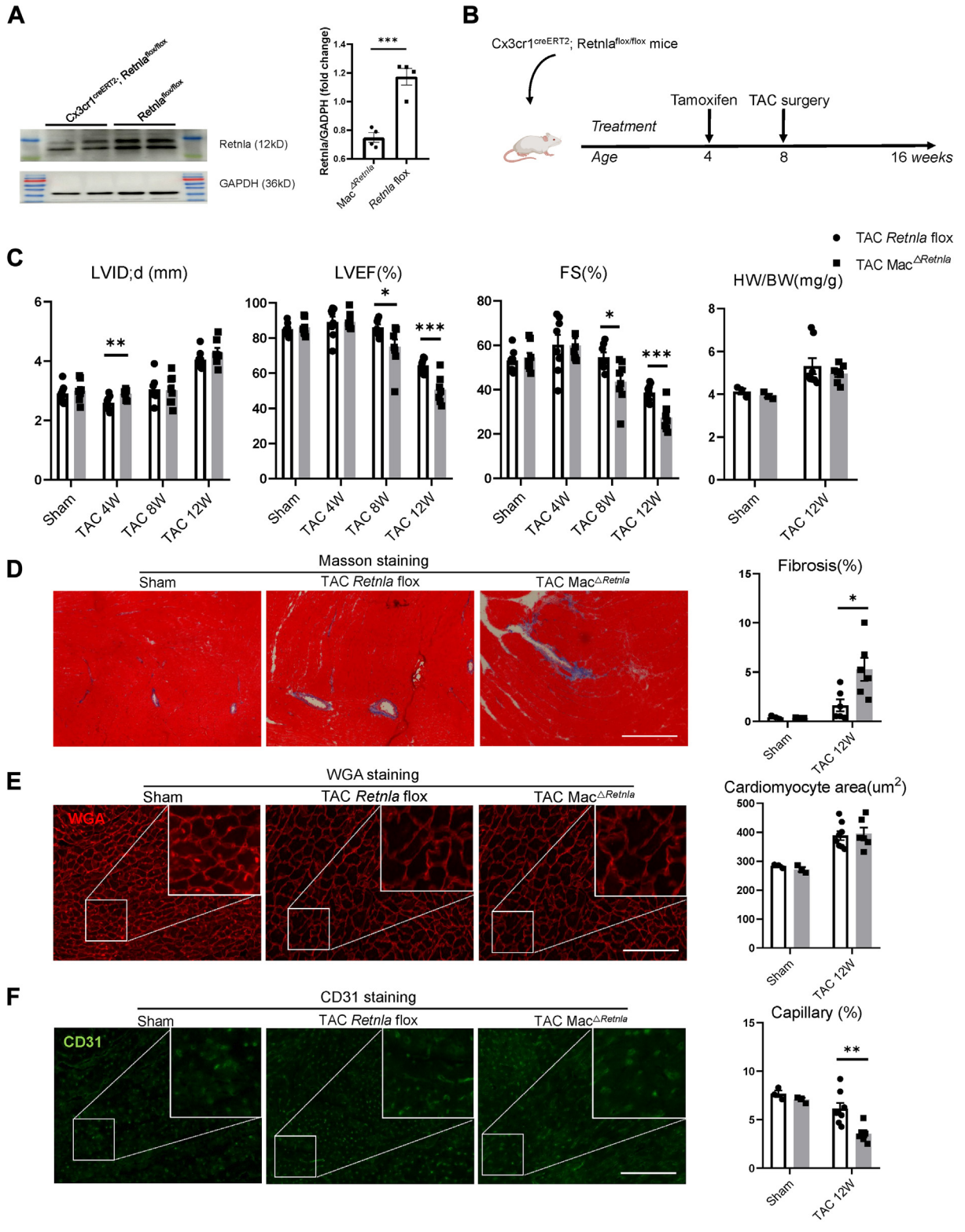

Continued on the next page

studies,[16,21] we applied different approaches and went further to describe the dynamics of this subgroup of macrophages systemically. We then carefully characterized the biological properties of these DP macrophages. We demonstrated that DP macrophages acted mainly as resident macrophages with minimal input from circulating monocytes, sharing similar dynamics with the TIMD4^{hi} macrophage subset in a steady state. This DP macrophage subset exhibited unique dynamics during our pressure overload-induced cardiac remodeling process. Unlike Lyve1^{hi} or MHCII ^{hi} macrophages, DP macrophages showed a decrease in their numbers at the late heart failure stage. Thus, our data have added different layers of information to the resident macrophages that have not been reported previously.[10,14,33] In addition, we have provided the key data showing that the specific reduction of DP macrophages could lead to a facilitated heart failure process, further highlighting the essential roles of this particular macrophage subpopulation. On the other hand, although TIMD4^{hi} macrophages serve as an essential group of resident macrophages and their beneficial effects have already been validated in previous studies,[13,18-20,34] their population number did not change significantly at the late stage in our study when the cardiac function was impaired. Thus, our data highlight the essential role of DP macrophages, especially when heart failure progresses.

Moreover, using scRNA-seq analysis, we have revealed that *Retnla* is a specific gene expressed in DP macrophages. Further decrease in cardiac performance by selective loss of resident macrophage-derived *Retnla* and improved heart function with a recombinant RELMα (coded by *Retnla*) supplementation experiment both supported the essential role of this DP macrophage subset in the adverse cardiac remodeling process. Interestingly, research using the scRNA-seq approach revealed that peripheral nerve macrophages exhibit 2 macrophage subsets: *Retnla*$^{+}$*Mgl1*$^{+}$ in the epineurium and *Retnla*$^{-}$*Mgl1*$^{-}$ in the endurium.[35] Similar results have also been shown in the liver, lung, and intestine.[27,36-38] RELMα, initially identified in a mouse model of asthma and later named hypoxia-induced mitogenic factor (HIMF) under hypoxic conditions, has been extensively studied.[39] Although earlier investigations suggested detrimental roles for RELMα proteins because of their abundant expression in pathologic settings, recent studies have revealed their potential beneficial effects in maintaining metabolic homeostasis, reducing inflammation, and promoting angiogenesis.[23,27,36,39-41] Notably, previous in vitro research demonstrated that RELMα inhibits cardiac fibroblast migration by decreasing the expression of α-smooth muscle actin and collagen type I alpha 2 chains.[42] Our study further elucidated that, in the heart, RELMα was predominantly expressed by macrophages, especially the DP macrophages, and RELMα played a crucial role in preventing fibrosis formation and promoting angiogenesis. These findings provide insights into how resident macrophages exert beneficial effects under pathologic conditions.[43,44]

Human resistin is primarily produced by immune cells, particularly the macrophages and monocytes.[45] The role of resistin in metabolism has been extensively researched, and the consensus in both mouse and human studies is that resistin plays a detrimental role in the development of insulin resistance, atherosclerosis, and hypertension.[26,39,45,46] In our study, a higher level of resistin was associated with better cardiac performance in ischemic heart failure patients; this phenomenon was also observed in patients who underwent aortic valve replacement procedures where the improved cardiac performance after the intervention therapy was associated with increased plasma resistin level (**Figures 7J and 7K**). Meanwhile, we demonstrated a preventive role for *Retnla* when it was used in a rather earlier stage in a TAC-induced heart failure mouse model, which was associated with enhanced angiogenesis and less fibrotic process. Thus, our data also strongly suggest that resistin can be used to predict the prognosis of heart failure patients.[47] Further investigation is necessary to validate its potential clinical application.

FIGURE 6 Continued

(A) *Retnla* protein expression detected by Western blot of cultured bone marrow–derived macrophages from Cx3cr1^{CreERT2};Retnla$^{flox/flox}$ mice (Mac$^{\triangle Retnla}$) compared with Retnla$^{flox/flox}$ mice (*Retnla* flox). (B) Either the TAC or sham procedure was performed at 3 weeks after the completion of tamoxifen administration. (C) Cardiac morphology and function were measured by echocardiography at 8 and 12 weeks postsurgery (n = 7 or 8). (D-F) Fibrosis (measured by Masson staining; 5× field of view scale; scale bars: 300 μm), cardiac hypertrophy (measured by wheat germ agglutinin, 20× field of view; scale bar: 100 μm), and capillary (measured by CD31 staining; 20× field of view; scale bar: 100 μm) were assessed in sham-operated hearts and hearts obtained from mice at 17 weeks post-TAC, respectively. A total of 5 or 6 randomized visual fields were selected and analyzed for each heart and averaged (n = 6 or 7). All data are expressed as the mean ± standard error of the mean. Values were analyzed by using Student's *t*-test unless otherwise specified. *$P < 0.05$; **$P < 0.01$; ***$P < 0.001$. Abbreviations as in **Figures 1 to 4**.

FIGURE 7 RELMα Supplementation Prevented Heart Failure

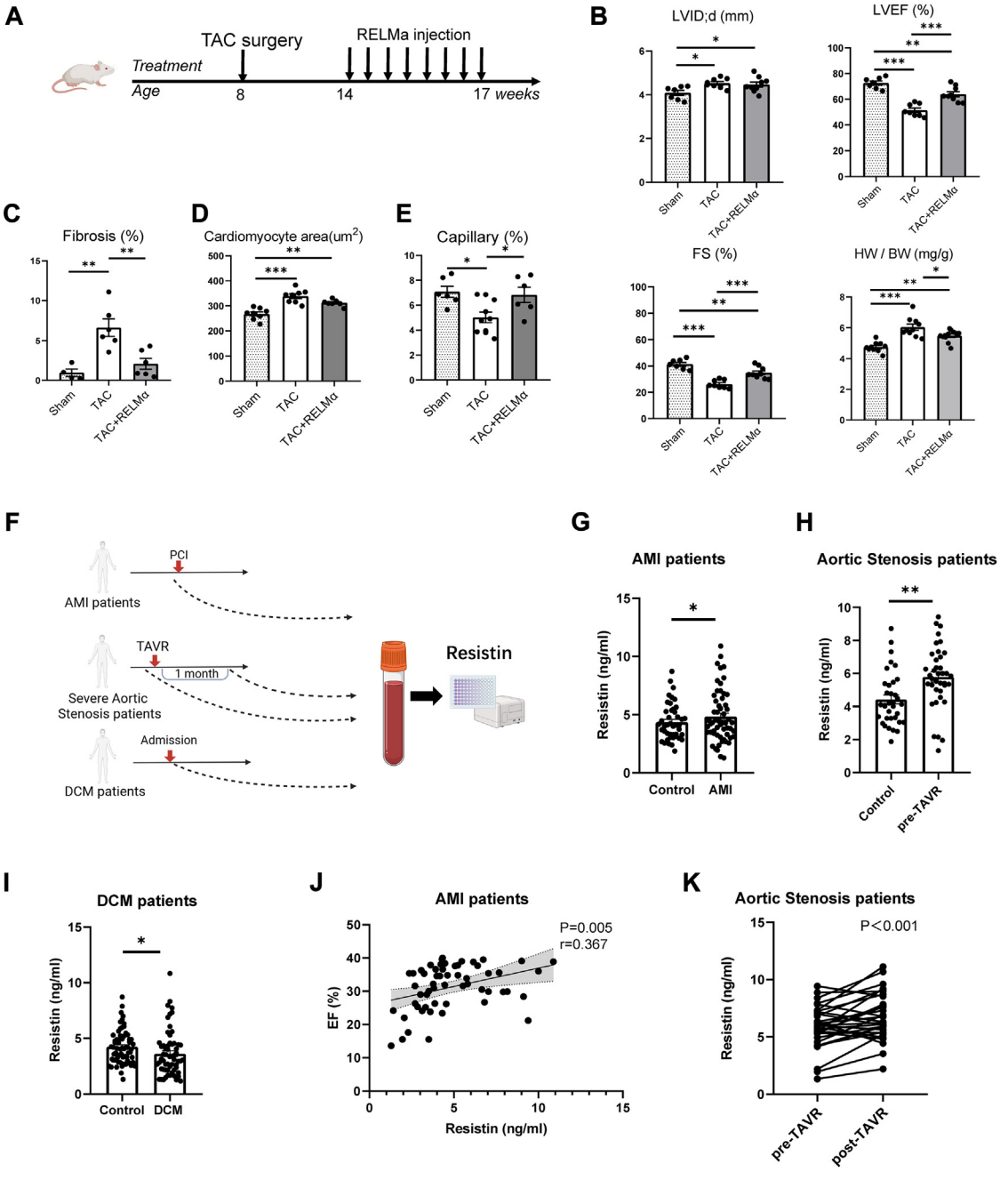

(A) Schematic of the protocol of RELMα therapy. Briefly, 8-week-old C57BL/6J mice received TAC surgery, and RELMα was given by intraperitoneal injection twice a week from 6 to 9 weeks post-TAC. (B) Cardiac morphology and function were measured by echocardiography at 9 weeks postsurgery (n = 7-9). (C to E) Fibrosis (measured by Masson staining), cardiac hypertrophy (measured by wheat germ agglutinin), and capillary (measured by CD31 staining) were assessed in sham-operated hearts and hearts obtained from mice at 17 weeks post-TAC, respectively (5-7 randomized visual fields were selected and analyzed for each heart and averaged; n = 4-7). Values in B through E were analyzed by using analysis of variance with Tukey post hoc analysis. (F) Plasma samples were collected among patients with severe aortic stenosis, AMI, and DCM. Resistin was detected using enzyme-linked immunosorbent assay. (G to I) The concentration of resistin in the plasma of patients and the age- and sex-matched control group. Values were analyzed by using Student's *t*-test. (J) Linear regression analysis was carried out to assess the association between the resistin concentration and the LVEF. (K) Resistin concentration before and 1 month after transcatheter aortic valve replacement surgery. Values were analyzed by using a paired Student's *t*-test. All the data are expressed as the mean ± SEM. $^{*}P < 0.05$; $^{**}P < 0.01$; $^{***}P < 0.001$. AMI = acute myocardial infarction; DCM = dilated cardiomyopathy; PCI = percutaneous coronary intervention; TAVR = transcatheter aortic valve replacement; other abbreviations as in Figures 1 to 4.

STUDY LIMITATIONS. There are certain limitations in the present study that we need to address. Our pseudotime trajectory analysis data indicated that DP macrophages might differentiate into MHCII^{hi} macrophages, strongly supporting that DP macrophages could simultaneously serve as intermediate cells during disease progression. A better orthogonal recombinase system should be developed to better label the different types of macrophage cells, which would provide precise information to help understand the biological function of these macrophages. In addition, the in vivo orthogonal recombinase system with Cre and Dre introduced by the AAV approach we used did not reach an ideal efficiency, resulting in only an approximately 30% decrease in the number of DP macrophages. Therefore, our conclusion is mainly based on this specific condition. A higher-efficiency system is undoubtedly needed to further test the effects following complete DP macrophage depletion, which might provide a different data set. Nevertheless, a slight decrease still resulted in a significant change in cardiac performance, strongly supporting the important roles of this special DP macrophage population.

CONCLUSIONS

We have successfully identified and validated the existence of a distinct macrophage subset, designated as DP macrophages, which exhibit unique origins and dynamics under both steady-state and pressure-overload stress conditions. These DP macrophages play a crucial role in preserving heart function by secreting RELMα. Our findings suggest that the current understanding of macrophage biology based on a dichotomous to trichotomous classification can be further expanded to a quarto classification by incorporating the novel DP macrophage subset. This advancement in classification will enhance our comprehension of macrophages' complex roles and functions in various physiologic and pathologic contexts.

ACKNOWLEDGMENTS The authors thank Linrong Lu (Zhejiang University School of Medicine) for helpful discussions. The authors are grateful for the technical support from Yingchao Wang (Zhejiang University) for TAC surgery.

FUNDING SUPPORT AND AUTHOR DISCLOSURES

This work was supported by grants from the National Natural Science Foundation of China (U22A20267, 82030014, to Dr J. Wang, 81970230 and 82370374 to Dr W. Zhu, U21A20338, 82370256 to Dr J. Chen). The authors have reported that they have no relationships relevant to the contents of this paper to disclose.

ADDRESS FOR CORRESPONDENCE: Dr Wei Zhu, Department of Cardiology, Second Affiliated Hospital, School of Medicine, 310000, No. 88 Jiefang Road, Shangcheng District, Hangzhou, Zhejiang, China. E-mail: weizhu65@zju.edu.cn. OR Dr Jian'an Wang, Department of Cardiology, Second Affiliated Hospital, School of Medicine, 310000, No. 88 Jiefang Road, Shangcheng District, Hangzhou, Zhejiang, China. E-mail: wangjianan111@zju.edu.cn.

PERSPECTIVES

COMPETENCY IN MEDICAL KNOWLEDGE: Heart failure is a severe and life-threatening disease that affects millions of people worldwide. The essential roles of macrophages have been increasingly recognized over the past decades in this process. Our present study explored the newly discovered resident TIMD4^{hi}MHCII^{hi} macrophages and their potential impact on heart function. Functional experiments have shown that TIMD4^{hi}MHCII^{hi} macrophages could modulate heart function by promoting angiogenesis and decreasing the formation of fibrosis. These findings highlight not only the biological function of the subpopulation of TIMD4^{hi}MHCII^{hi} macrophages but also the essential roles of *Retnla* in the pathologic process of heart failure.

TRANSLATIONAL OUTLOOK: Our research suggests that resistin may serve as a valuable indicator for the degree of decline in heart function in patients with AMI. Furthermore, resistin may be a predictive marker for heart function recovery post-TAVR. We must acknowledge that our observations did not find a correlation between resistin and heart function in DCM patients. These preliminary results warrant a further study to validate the role of resistin in patients with heart failure.

REFERENCES

1. Bleriot C, Chakarov S, Ginhoux F. Determinants of resident tissue macrophage identity and function. *Immunity*. 2020;52:957–970.

2. Watanabe S, Alexander M, Misharin AV, Budinger GRS. The role of macrophages in the resolution of inflammation. *J Clin Invest*. 2019;129:2619–2628.

3. Aurora AB, Porrello ER, Tan W, et al. Macrophages are required for neonatal heart regeneration. *J Clin Invest*. 2014;124:1382–1392.

4. Godwin JW, Pinto AR, Rosenthal NA. Macrophages are required for adult salamander limb regeneration. *Proc Natl Acad Sci U S A*. 2013;110:9415–9420.

5. Hulsmans M, Clauss S, Xiao L, et al. Macrophages facilitate electrical conduction in the heart. *Cell*. 2017;169:510–522.e520.

6. Yona S, Kim KW, Wolf Y, et al. Fate mapping reveals origins and dynamics of monocytes and tissue macrophages under homeostasis. *Immunity*. 2013;38:79–91.

7. Kolter J, Feuerstein R, Zeis P, et al. A subset of skin macrophages contributes to the surveillance and regeneration of local nerves. *Immunity*. 2019;50:1482–1497.e1487.

8. Gomez Perdiguero E, Klapproth K, Schulz C, et al. Tissue-resident macrophages originate from yolk-sac-derived erythro-myeloid progenitors. *Nature*. 2015;518:547–551.

9. Epelman S, Lavine KJ, Beaudin AE, et al. Embryonic and adult-derived resident cardiac macrophages are maintained through distinct mechanisms at steady state and during inflammation. *Immunity*. 2014;40:91–104.

10. Epelman S, Lavine KJ, Randolph GJ. Origin and functions of tissue macrophages. *Immunity*. 2014;41:21–35.

11. Correction for Lavine et al.. distinct macrophage lineages contribute to disparate patterns of cardiac recovery and remodeling in the neonatal and adult heart. *Proc Natl Acad Sci U S A*. 2016;113:E1414.

12. Bajpai G, Bredemeyer A, Li W, et al. Tissue resident CCR2- and CCR2+ cardiac macrophages differentially orchestrate monocyte recruitment and fate specification following myocardial injury. *Circ Res*. 2019;124:263–278.

13. Dick SA, Macklin JA, Nejat S, et al. Self-renewing resident cardiac macrophages limit adverse remodeling following myocardial infarction. *Nat Immunol*. 2019;20:29–39.

14. Liao X, Shen Y, Zhang R, et al. Distinct roles of resident and nonresident macrophages in nonischemic cardiomyopathy. *Proc Natl Acad Sci U S A*. 2018;115:E4661–E4669.

15. Patel B, Bansal SS, Ismahil MA, et al. CCR2(+) monocyte-derived infiltrating macrophages are required for adverse cardiac remodeling during pressure overload. *JACC Basic Transl Sci*. 2018;3:230–244.

16. Zaman R, Hamidzada H, Kantores C, et al. Selective loss of resident macrophage-derived insulin-like growth factor-1 abolishes adaptive cardiac growth to stress. *Immunity*. 2021;54:2057–2071.e2056.

17. Bajpai G, Schneider C, Wong N, et al. The human heart contains distinct macrophage subsets with divergent origins and functions. *Nat Med*. 2018;24:1234–1245.

18. Chakarov S, Lim HY, Tan L, et al. Two distinct interstitial macrophage populations coexist across tissues in specific subtissular niches. *Science*. 2019;363:eaau0964. https://doi.org/10.1126/science.aau0964

19. Cho CH, Koh YJ, Han J, et al. Angiogenic role of LYVE-1-positive macrophages in adipose tissue. *Circ Res*. 2007;100:e47–e57.

20. Lim HY, Lim SY, Tan CK, et al. Hyaluronan receptor LYVE-1-expressing macrophages maintain arterial tone through hyaluronan-mediated regulation of smooth muscle cell collagen. *Immunity*. 2018;49:326–341.e327.

21. Dick SA, Wong A, Hamidzada H, et al. Three tissue resident macrophage subsets coexist across organs with conserved origins and life cycles. *Sci Immunol*. 2022;7:eabf7777. https://doi.org/10.1126/sciimmunol.abf7777

22. Zaw AM, Williams CM, Law HK, Chow BK. Minimally invasive transverse aortic constriction in mice. *J Vis Exp*. 2017;(121):55293. https://doi.org/10.3791/55293

23. Sutherland TE, Ruckerl D, Logan N, et al. Ym1 induces RELMalpha and rescues IL-4Ralpha deficiency in lung repair during nematode infection. *PLoS Pathog*. 2018;14:e1007423. https://doi.org/10.1371/journal.ppat.1007423

24. Gerlach BD, Ampomah PB, Yurdagul A Jr, et al. Efferocytosis induces macrophage proliferation to help resolve tissue injury. *Cell Metab*. 2021;33:2445–2463.e2448.

25. Raes G, De Baetselier P, Noël W, et al. Differential expression of FIZZ1 and Ym1 in alternatively versus classically activated macrophages. *J Leukoc Biol*. 2002;71:597–602.

26. Steppan CM, Brown EJ, Wright CM, et al. A family of tissue-specific resistin-like molecules. *Proc Natl Acad Sci U S A*. 2001;98:502–506.

27. Tilg H, Moschen AR. Adipocytokines: mediators linking adipose tissue, inflammation and immunity. *Nat Rev Immunol*. 2006;6:772–783.

28. Kumamoto Y, Camporez JPG, Jurczak MJ, et al. CD301b(+) mononuclear phagocytes maintain positive energy balance through secretion of resistin-like molecule alpha. *Immunity*. 2016;45:583–596.

29. Swirski FK, Nahrendorf M. Cardioimmunology: the immune system in cardiac homeostasis and disease. *Nat Rev Immunol*. 2018;18:733–744.

30. Ma Y, Mouton AJ, Lindsey ML. Cardiac macrophage biology in the steady-state heart, the aging heart, and following myocardial infarction. *Transl Res*. 2018;191:15–28.

31. Leid J, Carrelha J, Boukarabila H, et al. Primitive embryonic macrophages are required for coronary development and maturation. *Circ Res*. 2016;118:1498–1511.

32. Nicolas-Avila JA, Lechuga-Vieco AV, Esteban-Martinez L, et al. A network of macrophages supports mitochondrial homeostasis in the heart. *Cell*. 2020;183:94–109.e123.

33. Hulsmans M, Sager HB, Roh JD, et al. Cardiac macrophages promote diastolic dysfunction. *J Exp Med*. 2018;215:423–440.

34. Pinto AR, Paolicelli R, Salimova E, et al. An abundant tissue macrophage population in the adult murine heart with a distinct alternatively-activated macrophage profile. *PLoS One*. 2012;7:e36814. https://doi.org/10.1371/journal.pone.0036814

35. Ydens E, Amann L, Asselbergh B, et al. Profiling peripheral nerve macrophages reveals two macrophage subsets with distinct localization, transcriptome and response to injury. *Nat Neurosci*. 2020;23:676–689.

36. Krljanac B, Schubart C, Naumann R, et al. RELMα-expressing macrophages protect against fatal lung damage and reduce parasite burden during helminth infection. *Sci Immunol*. 2019;4:eaau3814. https://doi.org/10.1126/sciimmunol.aau3814

37. Pai S, Njoku DB. The role of hypoxia-induced mitogenic factor in organ-specific inflammation in the lung and liver: key concepts and gaps in knowledge regarding molecular mechanisms of acute or immune-mediated liver injury. *Int J Mol Sci*. 2021;22:2717. https://doi.org/10.3390/ijms22052717

38. Forman R, Logunova L, Smith H, et al. *Trichuris muris* infection drives cell-intrinsic IL4R alpha independent colonic RELMα+ macrophages. *PLoS Pathog*. 2021;17:e1009768. https://doi.org/10.1371/journal.ppat.1009768

39. Teng X, Li D, Champion HC, Johns RA. FIZZ1/RELMalpha, a novel hypoxia-induced mitogenic factor in lung with vasoconstrictive and angiogenic properties. *Circ Res*. 2003;92:1065–1067.

40. Pine GM, Batugedara HM, Nair MG. Here, there and everywhere: resistin-like molecules in infection, inflammation, and metabolic disorders. *Cytokine*. 2018;110:442–451.

41. Kumar S, Wang G, Liu W, et al. Hypoxia-induced mitogenic factor promotes cardiac hypertrophy via calcium-dependent and hypoxia-inducible factor-1α mechanisms. *Hypertension*. 2018;72:331–342.

42. Li Y, Dong M, Wang Q, et al. HIMF deletion ameliorates acute myocardial ischemic injury by promoting macrophage transformation to reparative subtype. *Basic Res Cardiol*. 2021;116:30. https://doi.org/10.1007/s00395-021-00867-7

43. Revelo XS, Parthiban P, Chen C, et al. Cardiac resident macrophages prevent fibrosis and stimulate angiogenesis. *Circ Res*. 2021;129:1086–1101.

44. Wong NR, Mohan J, Kopecky BJ, et al. Resident cardiac macrophages mediate adaptive myocardial remodeling. *Immunity*. 2021;54:2072–2088.e2077.

45. Schwartz DR, Lazar MA. Human resistin: found in translation from mouse to man. *Trends Endocrinol Metab*. 2011;22(7):259–265.

46. Jang JC, Chen G, Wang SH, et al. Macrophage-derived human resistin is induced in multiple helminth infections and promotes inflammatory monocytes and increased parasite burden. *PLoS Pathog*. 2015;11(1):e1004579. https://doi.org/10.1371/journal.ppat.1004579

47. Miyawaki N, Ishizu K, Shirai S, et al. Assessing potential risks of future redo transcatheter aortic valve replacement in Asian patients. *JACC Asia*. 2023;4(1):25–39.

KEY WORDS fate mapping, heart failure, resident macrophage, Retnla

APPENDIX For supplemental Material and Methods including tables and figures, please see the online version of this paper.